https://doi.org/10.1016/j.surfcoat.2018.07.030

Laser polishing of additive manufactured CoCr components for controlling their wettability characteristics

K.C. Yung[1], W.J. Wang[1 *], T.Y. Xiao[1], H.S. Choy[1], X.Y. Mo[1],

S.S. Zhang[1], Z.X. Cai[1]

(1. Department of Industrial and Systems Engineering, The Hong Kong Polytechnic University, Hung Hom, Kowloon, Hong Kong)

[*]Corresponding author. Tel.: 852-27666615; fax.: 852-23629787.

E-mail address: wendy.wang@polyu.edu.hk (W.J.WANG).

Postal address: Department of Industrial and Systems Engineering, The Hong Kong Polytechnic University, Hung Hom, Kowloon, Hong Kong.

Abstract

Laser polishing treatment on 3D printed metal components has attracted great attention due to the potential applications in the dental implant and jewelry fields. In this study, cobalt-chromium (CoCr) alloys were polished over an area of 3×3 mm^2 using a pulsed mode 70W fiber laser. The micromorphology, composition, surface roughness and contact angles of the polished samples were characterized using a scanning electron microscope with energy-dispersive X-ray spectroscopy (SEM/EDX), optical profiler and contact angle goniometer, respectively. The results indicate that argon, with a median flow rate of 6.0 l/min, is the most feasible shielding gas for CoCr oxidation prevention, while maintaining a precise oxidation prevention control system. The object distance is found to be a critical parameter affecting the surface quality, and enhanced surface quality (Sa) ≤1 μm is achieved at a laser defocusing distance (Df) of +6 mm. Apart from laser power, other parameters in the laser polishing treatment, including scanning velocity, flow rate, object distance and hatching space, have a similar influence on surface roughness and contact angles. On a hydrophobic surface, the contact angle increases with an increase in surface roughness, due to the laser polishing variation of the CoCr surface with different defocusing distances. However, the contact angle decreases when the surface roughness of a hydrophilic surface increases, as in the laser polishing variation of the CoCr surface with different powers. Consequently, the wettability of laser treated CoCr seems more likely to be in the Wenzel's state.

Keywords

CoCr alloy, laser polishing, surface roughness, contact angle, wettability

1. Introduction

Co-Cr alloys are widely used in dentistry for removable partial dentures. During the bone healing period, Co-Cr alloys, as internal fixation implants, can provide temporary support in bone fracture surgery [1-3]. Nowadays, dentures and artificial prostheses comprised of Co-Cr alloys are usually fabricated by selective laser melting (SLM), which is an additive manufacturing method [4-6]. Currently, miniaturization of products with curved surfaces and/or inner structures is one of the major focuses in medical and biotechnological applications. As the surface of 3D printed metal products is constructed by solidified metal droplets [7], the resolution of drop-based 3D printing techniques is dependent on the aspect ratio of the pillars. The resolution range of the 3D printed metal products is constrained to approximately 1mm due to printed material properties [8]. Therefore, a rough surface in additive manufactured components cannot satisfy the requirements for medical applications [9].

Consequently, polishing methods including mechanical, ultrasonic, ion-beam, and chemical polishing have been investigated [10, 11], however, some limitations exist in the nature of the processes, such as inconsistent quality in manufacturing, high labor intensity and time consuming [12]. Although mechanical polishing is an effective method to obtain a specular surface, components with complex inner structures are hard to access and polish.

Laser polishing was introduced several years ago, and a considerable number of studies have indicated the significant impact of Selective Laser Polishing (SLP) on the reduction of surface roughness [13-16]. With a number of advantages, such as high flexibility, non-contact polishing, high energy density and environmentally-friendliness, SLP is able to achieve a closer tolerance and finer microstructure on the surface of the products [17-19].

The surface quality depends on the numerical control of the parameters and types of laser beam used, which may also directly affect the functionality of the product, such as the wettability and surface texture of an implant material [20-22].

Co-Cr alloys polished by mechanical methods have been investigated for surface roughness and wettability of the resin and metal, and with the advanced polishing process developed, the surface roughness has decreased remarkably [23, 24]. However, the influences of surface roughness and contact angles can vary depending on the laser polishing parameters and the variation in their chemical composition and microstructure. The purpose of this study is to determine the optimal polishing parameters and specular surfaces of Co-Cr alloys by laser polishing. Further, the influences and mechanisms of the wettability of polished surfaces are also investigated.

2. Materials and experimental

2.1 Materials and preparation

Additive manufactured CoCr components were printed in a uniform rectangular slab with dimensions of 100×75×8 mm^3 by a SLM 125 HL 3D Printer, with 400W power and in argon gas under an inert environment, assembled by SLM Solutions. The powders belong to the series CoCr/2.4979/F75 with different chemical composition, and the powder size was about 10~45 μm, as shown in table 1. The surface layer of the metal sample was combined into several layers of powder with a slice thickness of 0.025mm by the laser sintering process. The direction of the printed lines in each layer was perpendicular to each other. The scanning velocity of the laser beam was about 450mm/s.

Optical pulses were delivered by a fiber laser pulse application system (70W wavelength 1064nm produced by the SPI Laser) and were forwarded to a galvo-scanner (model F75

BEC). For the laser head, the ProSeries 1 14mm 2-Axis scan head and the beryllium mirrors with a reflective coating were provided by Cambridge Technology. For the focusing lens, an F-Theta lens provided by Linos was installed in the scan head with a focal length=160mm, while the laser beam of wavelength 1064nm was used. The pulse frequency and pulse duration of the fiber laser were 1000 KHz and 240 ns respectively. The 70W fiber laser was used for polishing the 3D printed CoCr.

The influence of the laser control and gas flux control parameters on the surface roughness and contact angles of the CoCr laser treatment were investigated. Laser power (W), scanning velocity (mm/s) and hatching space (mm) were the laser control parameters. The type of the shielding gas and the flow rate (l/min) were the gas flux control parameters. The gas cylinders of nitrogen and argon were installed with pressure regulators and pressure gauges, where the pressure of the released gas and the remaining gas capacity can be controlled and indicated respectively. To measure the gas flow rate more accurately, a numeric flow meter was placed between the one way flow control valve and the nozzle so as to be capable to determine the flow rate of the shielding gas with the room pressure instead of the pressure inside the gas cylinder.

In addition, the power of the laser beam could be adjusted while the surfaces of the metal samples were placed at a focusing distance (fd) of 210 mm. The focal plane was below to the working surface, with the defocusing distance (Df) defined as the distance from +2mm to +8mm measured from that focal plane, as shown in figure 1a. The hatching space [25] is defined as the distance or gap between neighboring laser scanned lines. It is another important parameter associated with the SLM process, as illustrated in figure 1b.

The one factor design of experiments can list all the combinations of all the factors, and address the changes in the different factors' levels. All the experiments using one factor design were thus carried out at ambient temperature (298-303 K), and conducted in terms of the parameters given in table 2 and table 3.

2.2 Characterization methods

Surface micromorphology was carried out using a JEOL Model JSM-6490 field emission scanning electron microscope (SEM). The contents of the oxidation were analyzed by a energy dispersive X-ray spectroscopy (EDX) detector, and the measurement error was about ±2%.

The surface roughness of the polished samples was measured by a Zygo white light interferometer system (Nexview optical surface profiler), which is a non-contact measurement system used to measure the profile and irregularity of an ultra-precision machined surface, and the measurement error was about ±10 nm. The arithmetic average roughness value (Ra) was used to quantify the roughness feature. The initial surface roughness was about 5 μm, as shown in figure 2.

The water contact angles and surface tension were tested by a contact angle goniometer, and ImageJ software with a Contact Angle Plug-in was used to calculate the contact angle captured by the goniometer, with a measurement error of about ±1°, as shown in figure 3. The aging effect was taken into consideration, so that all the water contact angles were tested within one week.

3. Results

3.1. Characterization of oxidition of post-laser treatment CoCr

Figure 4 illustrates the oxidation of CoCr with different types of shielding gas. The oxidation of CoCr with nitrogen tends to decrease and then remains stable when the flow rate of nitrogen is increasing. Comparatively, the extent of oxidation of CoCr with argon is lower, with a similar trend, and the EDX mappings shown in figure 4b and 4c have a lower oxidation. This reflects that the effectiveness of the oxidation prevention by argon is higher than that of nitrogen in the CoCr samples within a specific range of flow rate from 2.0 l/min to 10.0 l/min. It is observed that the extent of oxidation of polished CoCr without a shielding gas is lower than that of nitrogen shielding gas but higher than that of argon.

At a flow rate of 2.0 l/min, the volume of the shielding gas released is limited by the control valve. This means that a non-uniform distribution of the gas emission can occur through the nozzle used due to an insufficient supply of gas. As the flow rate increases to 6.0 l/min, a sufficient and even distribution of the shielding gas can be achieved from the gas cylinder. This leads to the low concentration of oxidation in the samples. For a flow rate over 6.0 l/min, widening the control valve allows more shielding gas to be released.

3.2. Surface roughness and contact angles with different gas flow rates

Figure 5 shows the roughness and contact angles of the samples under different atmospheres: air, nitrogen and argon. In general, the tendency of the surface roughness is increased first and then decreases while the flow rate is increasing. The best surface roughness is about 0.4 μm at 6.0 l/min flow rate when polished with argon. However, the highest surface roughness of the samples polished with argon and nitrogen at 2.0 l/min flow rate is about 0.7 μm and 0.6 μm, respectively. It is observed that the surface roughness of the polished samples in air (without shielding gas) is smaller than that with different shielding gases at 2.0 l/min flow rate, but is equal or worse than that at 6.0 and 10.0 l/min.

The change mentioned above can be caused by the change of gas volume released, since the flow rate is directly proportional to the gas volume consumption. It should be noted that the roughness shown in Fig. 5 is higher than when a low flow rate of inert gas (Argon) is introduced. The tests with N_2 gas result in lower roughness, and the roughness value is similar to the best result with Argon gas. It can be explained as follows: at a flow rate=2.0 l/min, the volume of the released shielding gas is limited by the control valve. This means that a non-uniform distribution of the gas emission can result in the nozzle due to the insufficient gas. The roughness values obtained at a flow rate=2.0 l/min by either N_2 gas or Argon gas were thus not in good distribution of gas control mode. At a low flow rate of 2.0 l/min, the sample with a low roughness value obtained by N_2 gas actually had more oxidation, and cannot be compared with the best result with Argon gas.

The contact angles of the samples under the shielding gas are larger than those without the shielding gas. The initial contact angle of the untreated CoCr is about 55°, and that of the laser treated CoCr without shielding gas is about 80°, while those of the laser treated CoCr with argon the shielding gas are about 94° to 101° at flow rates in the range of 2.0 to 10.0 l/min, and all of them are hydrophobic. Compared with CoCr without the shielding gas, the contact angle is increased by 26°. The contact angles of the samples with nitrogen are increased from 83.5° to 88.9°, with an increase in flow rate from 2.0 to 10.0 l/min, and all are obviously hydrophilic surfaces.

Consequently, taking surface oxidation, surface roughness and contact angles with different shielding gas into consideration, argon gas at a flow rate of 6.0 l/min is more suitable for the laser polishing of CoCr.

3.3. Surface roughness and contact angles with different object distances

In figure 6, the surface roughness of CoCr slightly decreases and then instantly increases, as the Df of the CoCr sample is approaching the focus distance (fd). The change of surface roughness of CoCr from Df +2 mm to fd is relatively small. The finest surface roughness that can be achieved by CoCr is about 0.45um at a Df of +6 mm, and a significant roughness reduction of 97% is obtained when compared to the surface roughness at a Df of +2 mm.

On the other hand, the most irregular surface is attained when Df is equal to fd. Irregularities are detected because of the insufficient power and scanning velocity during laser polishing. However, it is observed that a surface roughness lower than 1 μm can be obtained by defocusing with a low power fiber laser, which can provide an alternative solution for laser surface treatment.

The contact angles of the laser treated CoCr with different defocusing distances have a similar trend to that of roughness. The smallest contact angle is about 91°, and the largest is about 135°. Both are larger than that with no treatment and for laser treatment without a shielding gas for the CoCr surface. However, the required CoCr surface should be hydrophobic and smooth, which for the defocusing distance of +6 mm has the large contact angle of about 95° and the lowest roughness of about 0.45 μm.

3.4. Surface roughness and contact angles with different hatching spaces

In figure 7, the surface roughness of the CoCr samples rapidly decreases from the highest roughness of 0.9 μm to the lowest roughness of 0.45 μm as the hatching space increases from 0.01 mm to 0.05 mm. After a sudden drop, the surface roughness rises gradually to 0.96 μm when the hatching space increases further until reaching a hatching space of 0.09 mm. The difference between smallest and largest roughness is 0.55 μm,

which is much lower than that of the object distances, and means that the hatching space has far less impact than the object distance.

The contact angles of the laser treated CoCr with different hatching spaces have a similar trend to roughness, which decreases from the largest contact angle of 103° to the smallest contact angle of 95°, as the hatching space increases from 0.01 mm to 0.05 mm. The contact angle then increases slowly from 95° to 100° as the hatching space increases from 0.05 mm to 0.09 mm. However, the gap between the smallest contact angle of 95° and the largest angle of 103° , a small range of only 8°.

3.5. Surface roughness and contact angles with different scanning velocity

From figure 8, the change of surface roughness of the CoCr samples is plotted in a "V-shape" with an increase of scanning velocity from 100 mm/s to 1000 mm/s. The tendency of the surface roughness of the CoCr samples is that it sharply decreases from 1.9 μm to 0.61 μm and then slowly decreases to 0.45 μm as the scanning velocity increases from 100 mm/s to 300 mm/s and 500 mm/s, respectively. With the scanning velocity increasing from 500 mm/s to 1000 mm/s, the surface roughness rapidly increases to 2.5 μm, which indicates that the gap between the maximum and minimum surface roughness reaches 2.05 μm. The contact angles have a consistent variation with surface roughness, with a gap of 12° between the lowest at 94° at a scanning velocity of 500 mm/s and the largest at 106° at 1000 mm/s.

3.6. Surface roughness and contact angles with different laser power

It can be seen in figure 9 that the surface roughness of the CoCr samples instantly decreases from 4.976 μm to 0.45 μm as the percentage of laser power increases from 40 to 100, with corresponding increases in the contact angles from 80° to 94°. Only the surface

of the CoCr subjected to 100% laser power can be hydrophobic. Both trends are almost linear but inversely proportional.

Consequently, at a laser power of 70 W, scanning velocity 500 mm/s, hatching space 0.05 mm, defocusing distance +6 mm, and argon flow rate 6 l/min, the laser polished CoCr surface is appropriately hydrophobic and has minimum roughness. Almost all the parameters in the laser polishing treatment have a similar influence on surface roughness and contact angles, except for laser power. As there may be some optical output loss due to the thermal lens effect [26], the actual average power on the sample is expected to be lower. Obviously, the object distance has the largest effect on the surface roughness and contact angles. All of the underlying reasons associated with the results are discussed in the next section.

4. Discussion

The micromorphology of the untreated CoCr surface is shown in figure 10. It is observed that irregular waves and fluctuations, many small particles and black points exist. According to the EDX elements results, the black points have a very high carbon content. The small white particles have a similar weight percent of Cr and Co as the whole surface, and are the unmelted CoCr powders. The surfaces were shown to have a higher carbon concentration than expected, possibly due to surface contaminants as suggested by Vaithilingam et al [27].

Figure 11 shows the SEM images of the laser polished CoCr with different defocusing distances. There is no unmelted powder found, which means that the surface is remelted to a thin layer with laser polishing. It is found that there are rough, various size particles and porous micromorphologies at defocusing distance of +2 mm and at the focal plane. At

defocusing distances of +6 mm and +4 mm, orderly stripes are present on the surface, which are smoother than CoCr at +2 mm and at focal plane. However, there are many capillary cracks on the CoCr surface at +4 mm. At the defocusing distance of +8 mm, which is a large defocusing distance, many tiny peaks result from the low effective laser power and thin layer not being sufficiently remelted.

Different defocusing distances have the most influence on the roughness and contact angles. Because of the excessively high laser influence at the laser spot center, it is very easy to be evaporated into the pores. However, the laser influence has a relatively uniform distribution on the surface, away from the laser focus plane.

Figure 12 illustrates the optical profile of the laser polished CoCr with different defocusing distances. Different depth of peaks and valleys can be clearly observed. At an object distance of +8 mm, many tiny peaks and scanning lines appear. At an object distance of +4 mm, the depth of the scanning lines are deeper than CoCr at an object distance of +6 mm. At an object distance of +2 mm, there are deeper holes than the CoCr at focal plane. Consequently, the roughness and micromorphology are very different at varying object distances. Obviously, different energy levels are supplied by the laser equipment at different object distances. Rougher surfaces have higher surface energy, so the surface is in more unstable state and can easily become defective and corroded [28].

Different arc shaped water drops on the laser polished CoCr surface with different defocusing distances can be observed in figure 13. From the images, the angles increase when the object distance decreases from +8 mm to +2 mm. The CoCr surface with laser polishing at +8 mm, is hydrophilic surface and the contact angles are less than 90°. The other surfaces are hydrophobic and the contact angles are larger than 90°.

Laser fluence describes the energy delivered per unit (or effective) area, commonly defined in units of J/cm^2. The laser fluence q $[J/cm^2]$ depends on parameters of laser pulse energy Q [J], laser peak power p [W], pulse duration N [s] and effective focal spot area D $[cm^2]$. To calculate laser fluence, equation (1) is used, as shown below,

$$q=Q/D=pN/D \quad (1)$$

There is some optical output loss during the thermal lens effect, and the actual average power on the sample is expected to be lower. Therefore, with increasing laser peak power, the laser fluence increases, the defocusing distance increases, and the focal spot area increases, which leads to a decrease in the laser fluence, which is the reason for the difference in the remelting ratios.

Figure 14 illustrates the different CoCr surfaces treated with different laser powers. It is found that the unmelted powders have an increasing remelting ratio with an increase in laser power. Further, the irregular waves and fluctuations are reduced significantly, and orderly stripes are formed as the laser power increases. In figure 14 (a), many white particles are observed, whose contents are consistent with the raw Co-Cr power tested by EDX. Simultaneously, the surface shown in figure 14 (d) becomes smoother and the remelting powder filled the stripe lines well. The relationship between the spot size of the laser and resulting melt pool size is given in Ma et al [29, 30]. The laser fluence on each surface has a great difference with varying laser power. The particular range of 1~3 J/mm^2, with lower laser fluence, can result in higher surface roughness and the enhanced wettability.

Figure 15 shows water drops on a laser polished CoCr surface at different powers. It is observed that the contact angles are about 80°, 85°, 89° and 94° respectively. The CoCr

surface with laser powers of 40% to 80% are hydrophilic, and only that of 100% is hydrophobic. High power has high surface energy, which has an effect on surface wettability. The oxide content also has a reduced variation with the increase of laser power. Indeed, the surface hydrophilicity can be altered chemically because of the affinity between the oxides and hydroxylation [31]. It is well known that the oxygen content of a metal surface is the reason for the increase in the wettability [32].

The selection of the hatching space has a strong relevance with the laser device spot diameter. The experimental laser equipment at the focus distance has a spot diameter of 0.05 mm. Clearly, in figure 16, the hatching space 0.01 mm represents the narrowest gap between the two stripes in five levels. With the hatching space increasing, the gaps become wider. It means that too small a hatching space will generate too many gaps, remelting lines and have overlapping results with prominent bumps. Both the gaps and bumps affect the surface roughness variation. However, a too large hatching space cannot achieve sufficient remelting and only a part of the entire surface remelts, which generates many bumps but not enough gaps. Consequently, the change of the remelting ratio depends on the hatching space, to a certain degree. The laser scanning velocity effects the surface heat loss rate, which is also a significant fluence factor.

Based on the work of adhesion and Gibbs free energy variation, equation (2) is formulated, which is derived from the Fowkes theoretical method [33, 34]. This equation is used to describe the adhesion possibility between a liquid and solid surface and W_a has a direct relation with the two neighboring phases. If the process can occur at constant temperature and isopiestic pressure spontaneously, ΔG should be equal or larger than zero. It means the system energy is reduced more, the absolute value of W_a is larger, and the

adhesion between the water and CoCr surface is firmer. When θ is increased from 90° to 180°, the work of adhesion is reduced, which means that the surface is hydrophobic and water drops do not firmly adhere to it. Also the same effect occurs when θ increases from 0° to 90°.

$$W_a=\Delta G=\gamma_{l\text{-}s} - \gamma_{l\text{-}g} -\gamma_{s\text{-}g}= - \gamma_{l\text{-}g}\,(1+\cos\theta) \quad (2)$$

The system energy is tightly associated with surface tension, and the work of adhesion, which is shown as $\gamma_{s\text{-}g}$. For a larger $\gamma_{s\text{-}g}$, the more hydrophilic the surface, the larger the surface energy. Consequently, a water drop on the CoCr surface is in a balanced state, a state with the smallest system energy, so that the surface energy decreases and becomes more stable with increase of laser power.

According to the Wenzel model, shown in figure 17, on the homogeneous roughness surface, equation (3) can be used to describe the contact angle. θ^* is the contact angle of the minimum system free energy and γ is the roughness ratio of the true area to the apparent area, which indicates how the surface roughness of a uniform surface is affected. θ is Young's contact angle of an ideal surface.

$$\cos\theta^*=\gamma\cos\theta \quad (3)$$

Because γ is always greater than 1, the contact angle increases with an increase in surface roughness for a hydrophobic surface, just like the variation of a laser polished CoCr surface with different defocusing amounts. However, the contact angle decreases when the roughness of a hydrophilic surface increases, as shown in the variation of the laser polished CoCr surface with different powers. Consequently, the wettability of laser treated CoCr appears more likely to be in the Wenzel state.

5. Conclusions

This study focuses on the laser polishing of additive manufactured CoCr surfaces. Based on the experimental investigation, the study optimizes the laser polishing parameters on additive manufactured CoCr materials, and the laser polishing process. The following conclusions are obtained:

(1) The laser polishing process can make thin section parts smooth and can significantly improve the surface quality of additive manufactured parts.

(2) Increases of the object distance and laser power have the largest effect on the surface quality, and the laser fluence cannot reflect the spot focus distance.

(3) The use of argon with an optimized flow rate during the laser polishing process improves the surface roughness and contact angles.

(4) The variation of surface roughness and contact angles can be explained by the Wenzel model.

In future research, for each parameter the individual weight function, regarding roughness and wettability will be studied in terms of the interactive relationship between these parameters in a more comprehensive design of experiment. Emphasis also will be put on a five axis laser polishing system to polish an additive manufactured component with complicated curve surfaces. On account of the remelting process in laser polishing, more analysis on the metallurgical and phase changes will be considered, such as hardness, magnetism and corrosion resistance.

Acknowledgement

This work was funded by the Hong Kong Innovation Technology Fund (ITF) under project number ITS/369/15.

References

[1] P. Muller, P. Mognol, J.Y. Hascoet, Modeling and control of a direct laser powder deposition process for Functionally Graded Materials (FGM) parts manufacturing, J Mater Process Tech 213(5) (2013) 685-692.

[2] N.A. Orchard, J.A. Howlett, E.H. Davies, G.J. Pearson, Adhesive composite resins for artificial teeth: a laboratory investigation of bond strength to a cobalt-chromium alloy, Biomaterials 18(13) (1997) 935-938.

[3] M.A. Vasylyev, V.A. Tinkov, V.S. Filatova, S.M. Voloshko, P.A. Gurin, Generation of the periodic surface structures on the dental Co–Cr–Mo alloy by Nd:YAG laser in an inert atmosphere, Appl. Surf. Sci. 258(10) (2012) 4424-4427.

[4] W.S. Gora, Y. Tian, A.P. Cabo, M. Ardron, R.R.J. Maier, P. Prangnell, N.J. Weston, D.P. Hand, Enhancing Surface Finish of Additively Manufactured Titanium and Cobalt Chrome Elements Using Laser Based Finishing, Phys. Procedia 83 (2016) 258-263.

[5] A. Takaichi, Suyalatu, T. Nakamoto, N. Joko, N. Nomura, Y. Tsutsumi, S. Migita, H. Doi, S. Kurosu, A. Chiba, N. Wakabayashi, Y. Igarashi, T. Hanawa, Microstructures and mechanical properties of Co–29Cr–6Mo alloy fabricated by selective laser melting process for dental applications, J. Mech. Behav. Biomed. 21 (2013) 67-76.

[6] J. Tu, K.-F. Zhou, Z.-M. Zhou, C. Huang, H.-L. Tang, Microstructural characteristics of cobalt treated by high-speed laser surface melting under high power, Mater. Charact. 128 (2017) 63-67.

[7] C.W. Visser, R. Pohl, C. Sun, G.W. Römer, B. Huis in ‘t Veld, D. Lohse, Toward 3D Printing of Pure Metals by Laser-Induced Forward Transfer, Adv. Mater. 27(27) (2015) 4087-4092.

[8] S.y. Zhong, L.h. Qi, J. Luo, H.s. Zuo, X.h. Hou, H.j. Li, Effect of process parameters on copper droplet ejecting by pneumatic drop-on-demand technology, J Mater Process Tech 214(12) (2014) 3089-3097.

[9] J.J. Adams, E.B. Duoss, T.F. Malkowski, M.J. Motala, B.Y. Ahn, R.G. Nuzzo, J.T. Bernhard, J.A. Lewis, Conformal Printing of Electrically Small Antennas on Three-Dimensional Surfaces, Adv. Mater. 23(11) (2011) 1335-1340.

[10] J.H. Jung, H.K. Park, B.S. Lee, J. Choi, B. Seo, H.K. Kim, G.H. Kim, H.G. Kim, Study on surface shape control of pure Ti fabricated by electron beam melting using electrolytic polishing, Surf.Coat Tech. 324(Supplement C) (2017) 106-110.

[11] E. Ukar, A. Lamikiz, F. Liébana, S. Martínez, I. Tabernero, An industrial approach of laser polishing with different laser sources, Mat. Sci. Eng. A-Struct. 46(7) (2015) 661-667.

[12] E.V. Bordatchev, A.M.K. Hafiz, O.R. Tutunea Fatan, Performance of laser polishing in finishing of metallic surfaces, Int. J. Adv. Manuf. Tech. 73(1) (2014) 35-52.

[13] M.M. Pariona, V. Teleginski, K.d. Santos, E.L.R. dos Santos, A.A.d.O.C. de Lima, R. Riva, AFM study of the effects of laser surface remelting on the morphology of Al–Fe aerospace alloys, Mater. Charact. 74 (2012) 64-76.

[14] D. Bhaduri, P. Penchev, A. Batal, S. Dimov, S.L. Soo, S. Sten, U. Harrysson, Z. Zhang, H. Dong, Laser polishing of 3D printed mesoscale components, Appl. Surf. Sci. 405 (2017) 29-46.

[15] T.M. Shao, M. Hua, H.Y. Tam, E.H.M. Cheung, An approach to modelling of laser polishing of metals, Surf.Coat Tech. 197(1) (2005) 77-84.

[16] I. Gnilitskyi, V. Gruzdev, N.M. Bulgakova, T. Mocek, L. Orazi, Mechanisms of high-regularity periodic structuring of silicon surface by sub-MHz repetition rate ultrashort laser pulses, Appl. Phys. Lett. 109 (2016) 143101

[17] R. Avilés, J. Albizuri, E. Ukar, A. Lamikiz, A. Avilés, Influence of laser polishing in an inert atmosphere on the high cycle fatigue strength of AISI 1045 steel, Int. J. Fatigue 68 (2014) 67-79.

[18] T.L. Perry, D. Werschmoeller, X. Li, F.E. Pfefferkorn, N.A. Duffie, Pulsed laser polishing of micro-milled Ti6Al4V samples, J. Manuf. Process. 11(2) (2009) 74-81.

[19] A.Lamikiz, J.A.Sánchez, L.N. López de Lacalle, J.L.Arana, Laser polishing of parts built up by selective laser sintering, Int. J. Mach. Tool. Manuf. 47(12) (2007) 2040-2050.

[20] K.J. Kubiak, M.C.T. Wilson, T.G. Mathia, P. Carval, Wettability versus roughness of engineering surfaces, Wear 271(3) (2011) 523-528.

[21] N.B. Dahotre, S.R. Paital, A.N. Samant, C. Daniel, Wetting behaviour of laser synthetic surface microtextures on Ti–6Al–4V for bioapplication, P. Roy. Soc. A-Math. Phy. Eng. Sci. 368(1917) (2010) 1863.

[22] Z. Yang, Y.L. Tian, C.J. Yang, F.J. Wang, X.P. Liu, Modification of wetting property of Inconel 718 surface by nanosecond laser texturing, Appl. Surf. Sci. 414 (2017) 313-324.

[23] M. Nishioka, Y. Yamabe, K. Hisatsune, H. Fujii, Influence of Polishing of Denture Base Resin and Metal Surfaces on Wettability with Water and Saliva, Dent. Mater. J. 25(1) (2006) 161-165.

[24] I. Yoda, H. Koseki, M. Tomita, T. Shida, H. Horiuchi, H. Sakoda, M. Osaki, Effect of surface roughness of biomaterials on Staphylococcus epidermidis adhesion, BMC Microbiol. 14(1) (2014) 234.

[25] C.Y. Yap, C.K. Chua, Z.L. Dong, Z.H. Liu, D.Q. Zhang, L.E. Loh, S.L. Sing, Review of selective laser melting: Materials and applications, Appl. Phys. Rev. 2(4) (2015) 041101.

[26] D.L. Kim, B.T. Kim, Laser output power losses in ceramic Nd:YAG lasers due to thermal effects, Optik 127(20) (2016) 9738-9742.

[27] J. Vaithilingam, S. Kilsby, R.D. Goodridge, S.D.R. Christie, S. Edmondson, R.J.M. Hague, Immobilisation of an antibacterial drug to Ti6Al4V components fabricated using selective laser melting, Appl. Surf. Sci. 314 (2014) 642-654.

[28] B. Evgeny, T. Hughes, D. Eskin, Effect of surface roughness on corrosion behaviour of low carbon steel in inhibited 4M hydrochloric acid under laminar and turbulent flow conditions, Corros. Sci. 103 (2016) 196-205.

[29] C. Ma, M. Vadali, N.A. Duffie, F.E. Pfefferkorn, X.C. Li, Melt Pool Flow and Surface Evolution During Pulsed Laser Micro Polishing of Ti6Al4V, J. Manuf. Sci. Eng. 135(6) (2013) 061023.

[30] B.C. Zhang, H.L. Liao, C. Coddet, Effects of processing parameters on properties of selective laser melting Mg-9%Al powder mixture, Mater. Design 34 (2012) 753-758.

[31] M.M. Gentleman, J.A. Ruud, Role of Hydroxyls in Oxide Wettability, Langmuir 26(3) (2010) 1408-1411.

[32] A.M. Kietziga, M.N. Mirvakilia, S. Kamalb, P. Englezosa, S.G. Hatzikiriakosa, Nanopatterned Metallic Surfaces: Their Wettability and Impact on Ice Friction, J. Adhes. Sci. Technol. 25(12) (2011) 1293-1303.

[33] B. Jańczuk, T. Białłopiotrowicz, Surface free-energy components of liquids and low energy solids and contact angles, J. Colloid. Interf. Sci. 127(1) (1989) 189-204.

[34] F.M. Fowkes, attractive forces at interfaces, Ind. Eng. Chem. 56(12) (1964) 40-52.

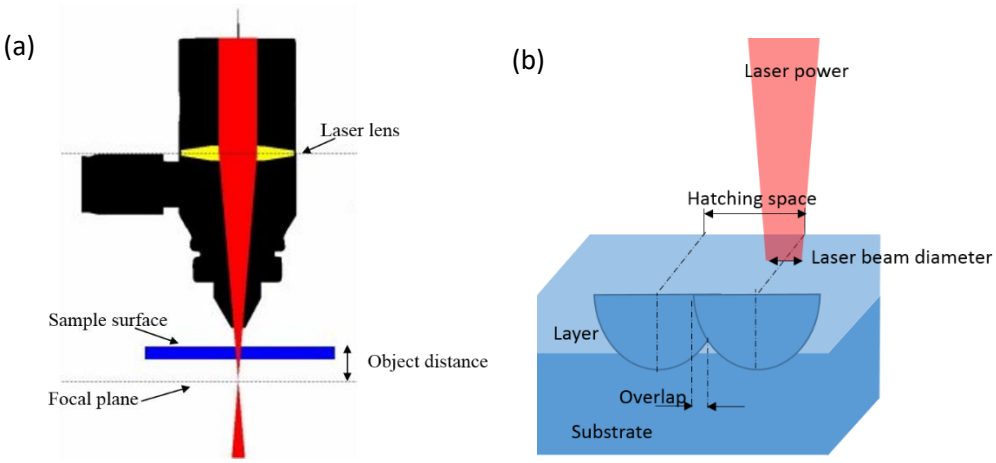

Figure 1

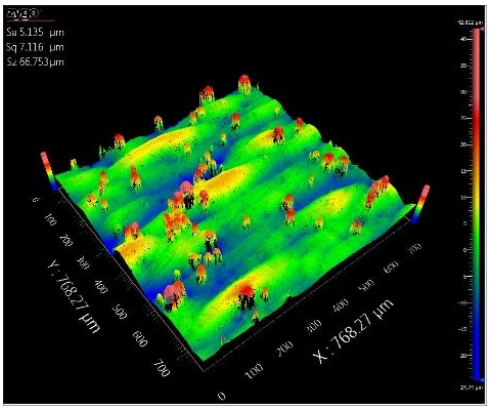

Figure 2

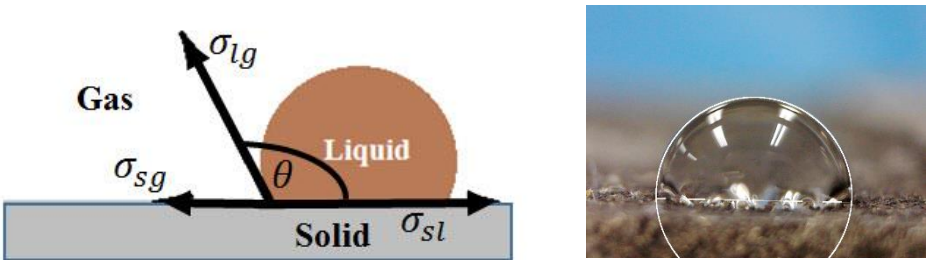

Figure 3

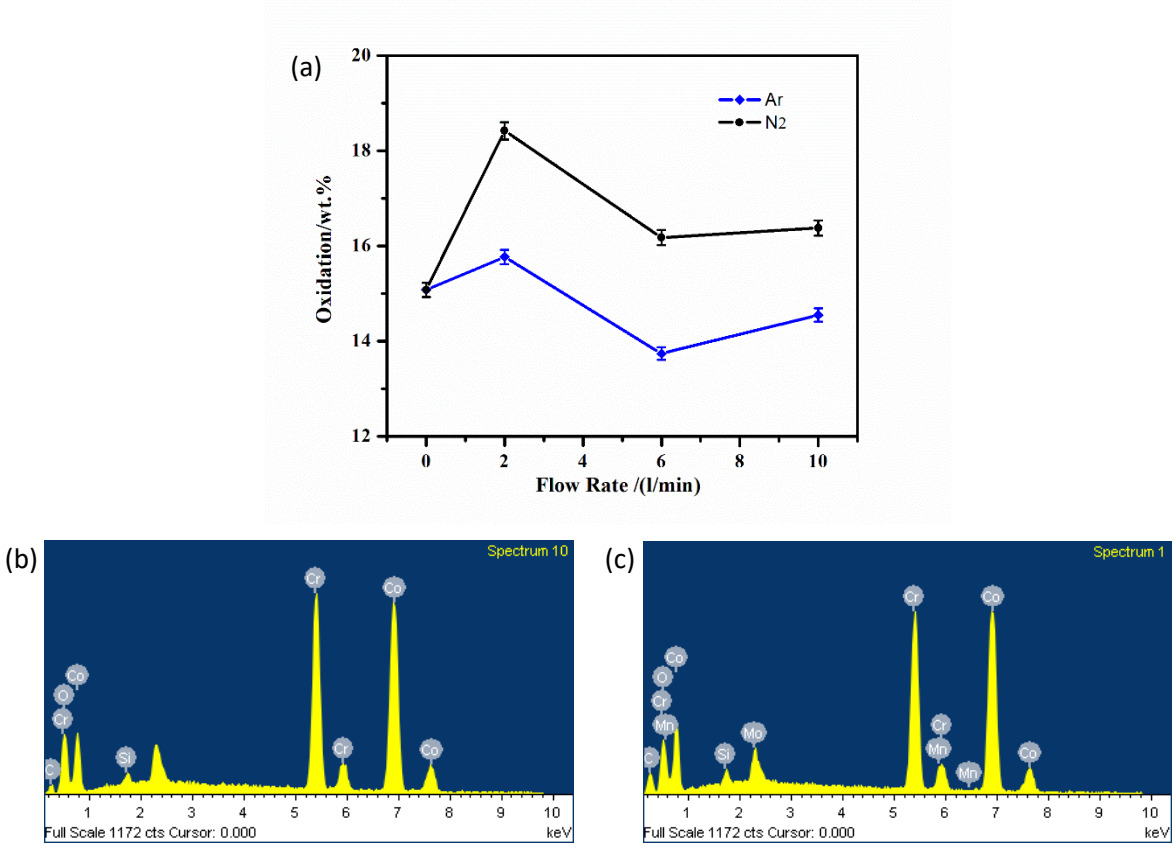

Figure 4

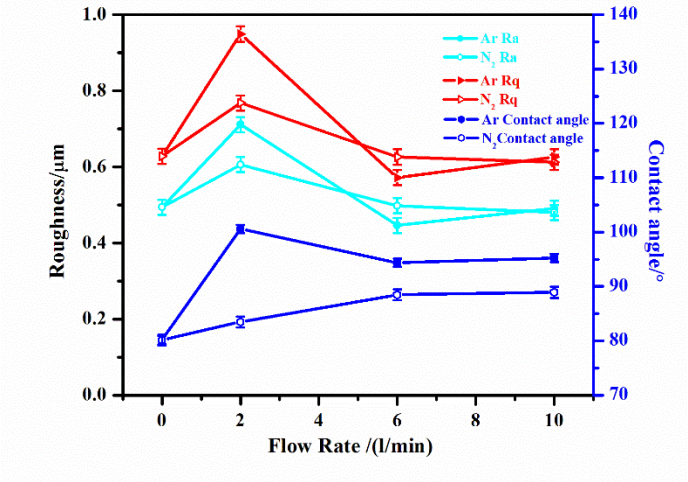

Figure 5

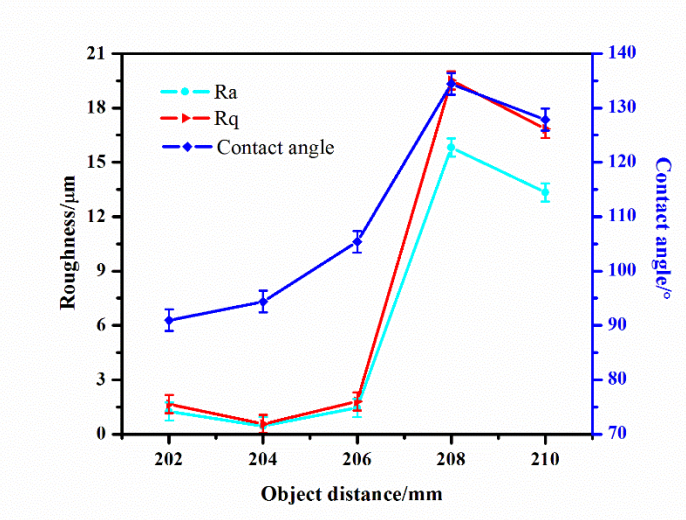

Figure 6

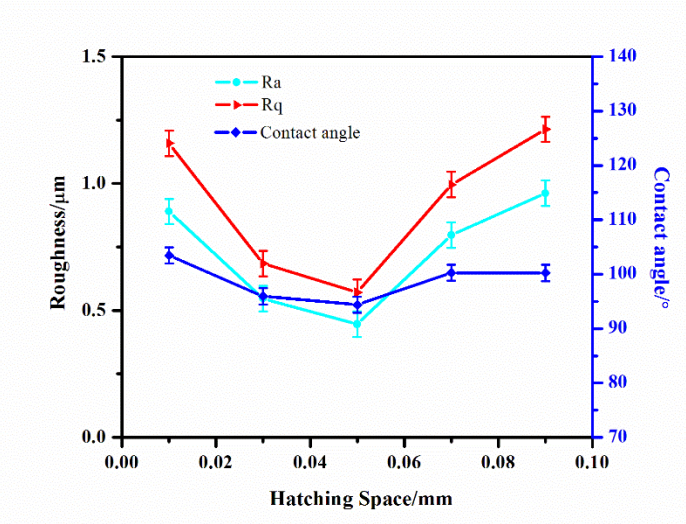

Figure 7

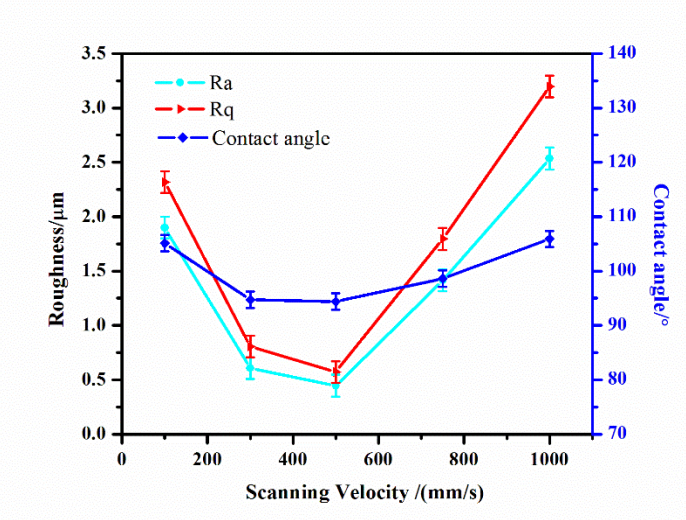

Figure 8

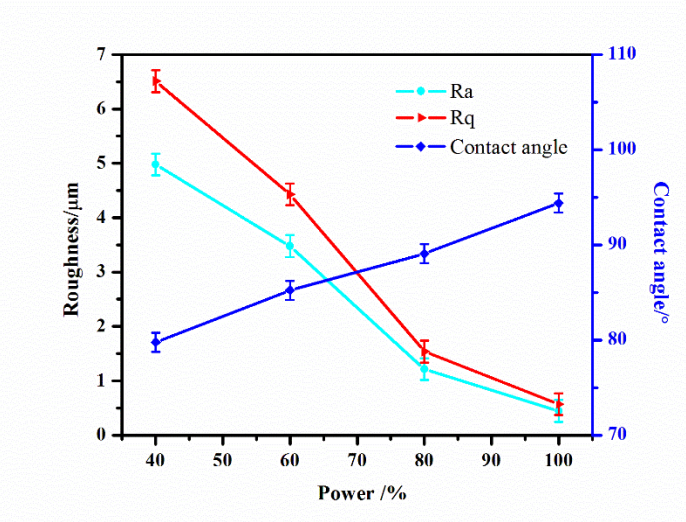

Figure 9

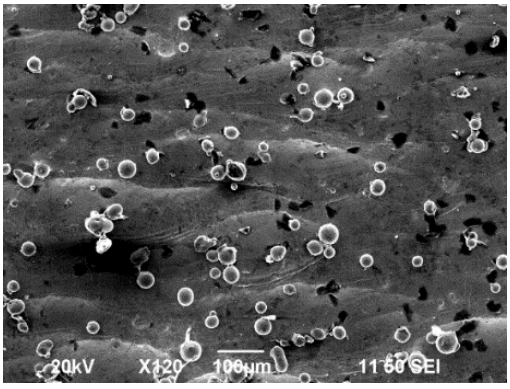

Figure 10

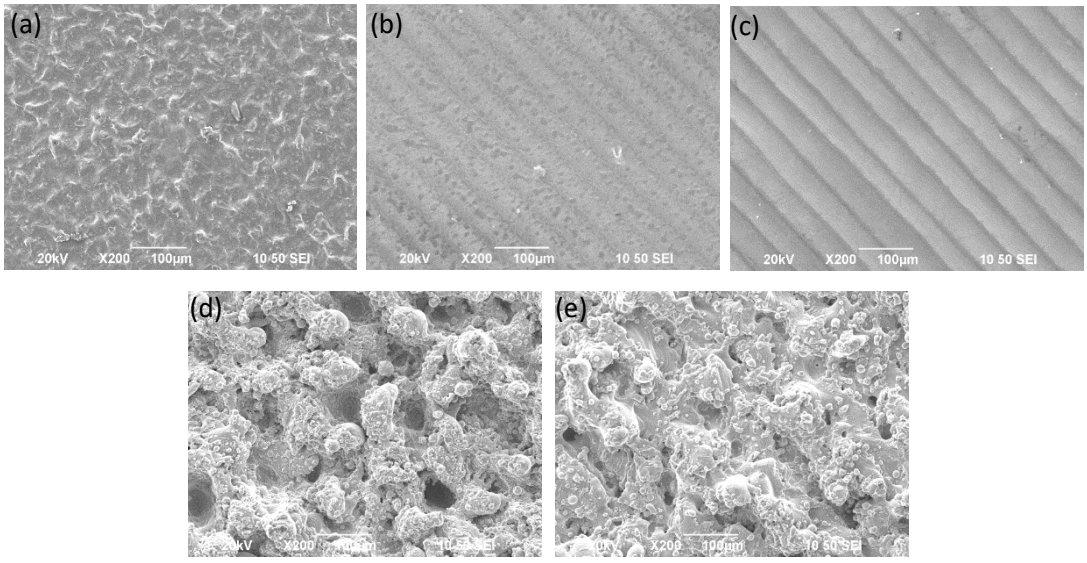

Figure 11

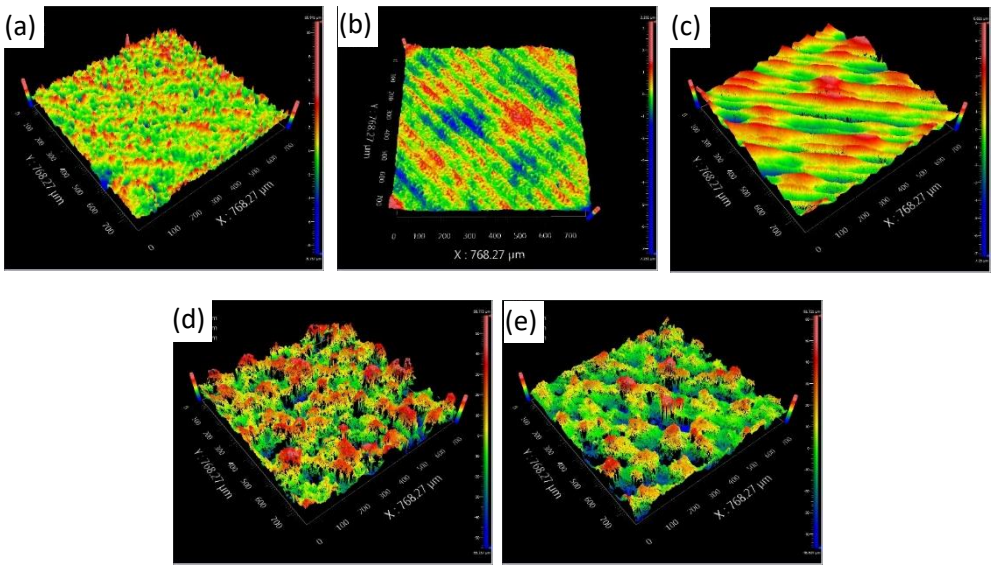

Figure 12

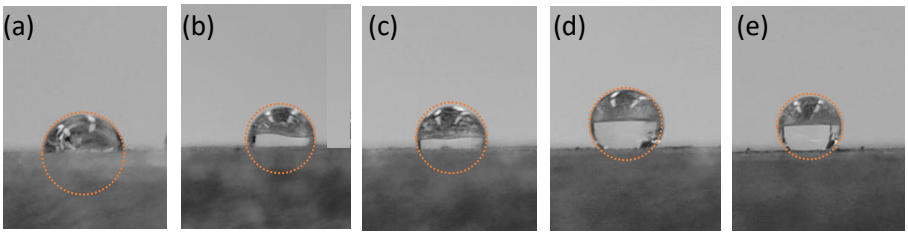

Figure 13

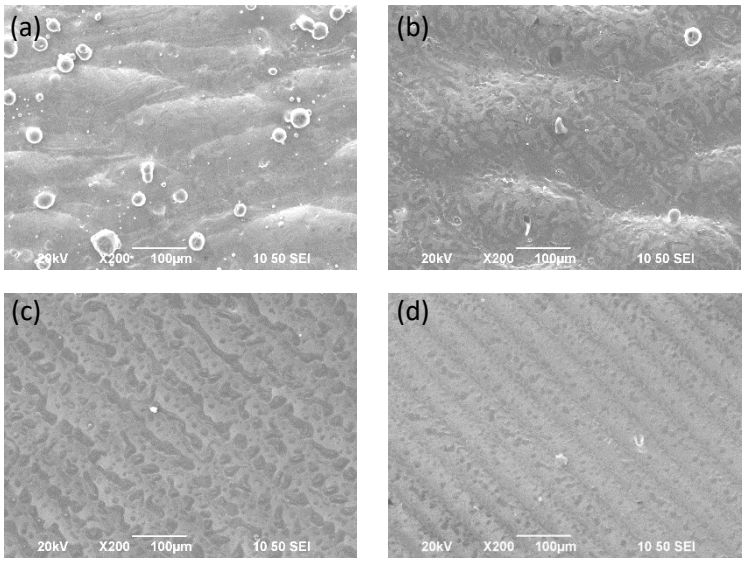

Figure 14

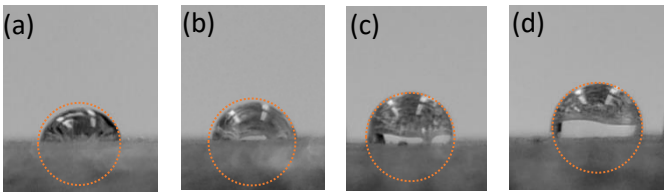

Figure 15

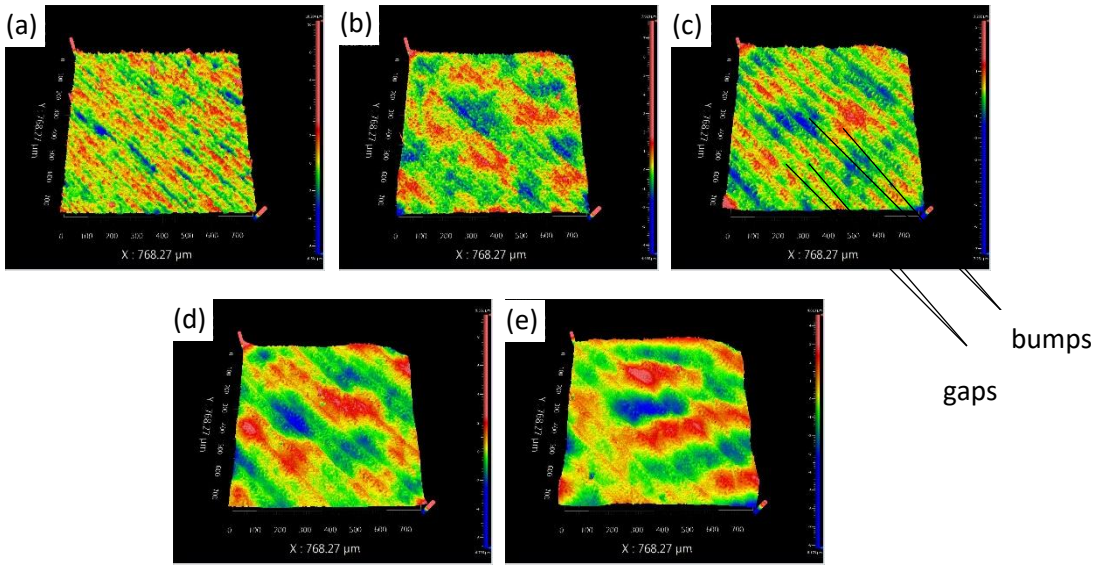

Figure 16

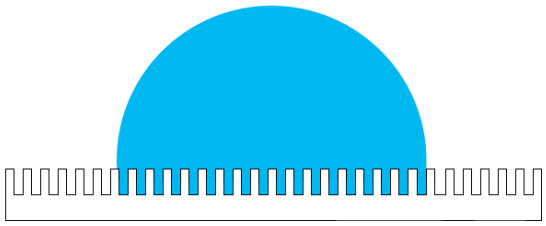

Figure 17

Table 1 Compositions of 3d printing powders of cobalt-chromium (CoCr)

Composition (wt.%)	Cobalt-chromium Alloy (CoCr)
Co	60.00-68.00
Cr	27.00-30.00
Al	<0.01
B	<0.01
C	<0.01
Fe	<0.75
Mn	<1.00
Mo	5.00-7.00
N	<0.25
Ni	<0.50
P	<0.02
S	<0.01
Si	<1.00
Ti	<0.10
W	<0.20

Table 2 Levels and factors of laser polishing parameters

Laser power ×70w	scanning velocity mm/s	hatching space mm	flow rate l/min	Object distances mm
40	100	0.01	0	+8
60	300	0.03	2	+6
80	500	0.05	6	+4
100	800	0.07	10	+2
—	1000	0.09	—	0

The parameters highlighted in red are unchanged when other factors changed.

Table 3 Laser parameters employed during surface processing

Parameter	Value
Wavelength (nm)	1064
Pulse duration (ns)	240
Maximum pulse repetition frequency (KHz)	1000
Maximum pulse energy, Emax (mJ)	1
Typical peak power at Emax (kW)	13
Beam spot size (μm)	50